Structural Fluctuation Governed Dynamic Diradical Character in Pentacene

Hongfang Yang, Mengzhen Chen, Xinyu Song*, Yuxiang Bu

School of Chemistry and Chemical Engineering, Shandong University, Jinan, 250100,

People's Republic of China

The Corresponding Authors: songxy@sdu.edu.cn

Electronic Supplementary Materials

Contents

1. The Complete Citation for Ref. 36

Frisch, M. J.; Trucks, G. W.; Schlegel, H. B.; Scuseria, G. E.; Robb, M. A.; Cheeseman, J. R.; Montgomery, J. A., Jr; ; Vreven, T.; Kudin, K. N.; Burant, J. C.; Millam, J. M.; Iyengar, S. S.; Tomasi, J.; Barone, V.; Mennucci, B.; Cossi, M.; Scalmani, G.; Rega, N.; Petersson, G. A.; Nakatsuji, H.; Hada, M.; Ehara, M.; Toyota, M.; Fukuda, R.; Hasegawa, J.; Ishida, M.; Nakajima, T.; Honda, Y.; Kitao, O.; Nakai, H.; Klene, M.; Li, X.; Knox, J. E.; Hratchian, H. P.; Cross, J. B.; Adamo, C.; Jaramillo, J.; Gomperts, R.; Stratmann, R. E.; Yazyev, O.; Austin, A. J.; Cammi, R.; Pomelli, C.; Ochterski, J. W.; Ayala, P. Y.; Morokuma, K.; Voth, G. A.; Salvador, P.; Dannenberg, J. J.; Zakrzewski, V. G.; Dapprich, S.; Daniels, A. D.; Strain, M. C.; Farkas, O.; Malick, D. K.; Rabuck, A. D.; Raghavachari, K.; Foresman, J. B.; Ortiz, J. V.; Cui, Q.; Baboul, A. G.; Clifford, S.; Cioslowski, J.; Stefanov, B. B.; Liu, G.; Liashenko, A.; Piskorz, P.; Komaromi, I.; Martin, R. L.; Fox, D. J.; Keith, T.; Al-Laham, M. A.; Peng, C. Y.; Nanayakkara, A.; Challacombe, M.; Gill, P. M. W.; Johnson, B.; Chen, W.; Wong, M. W.; Gonzalez, C.; Pople, J. A. *Gaussian 03*; Gaussian, Inc.: Wallingford, CT, **2004**.

2. Calculational Details

In order to explore potential diradical character and relevant dynamic properties of pentacene, we performed an *ab initio* molecular dynamics (AIMD) simulation for one pentacene molecule.   In our AIMD simulation, we used the DMol^3 package which is based on the density-functional theory (DFT).   Before AIMD simulation, a pentacene molecule was firstly optimized to obtain its initial configuration (static structure) using a double numeric plus polarization basis (DNP) set and the generalized gradient approximation (GGA) proposed by Perdew-Burke-Ernzerhof (PBE) for the exchange and correlation function.   During the geometry optimization, all electrons are included in the spin-unrestricted calculation.   The same conditions were maintained in the AIMD simulation.   Besides, total AIMD simulation time is 2 ps, which was performed within the canonical (NVT) ensemble with the system temperature around 300 K by using the Nose-Hoover chain of thermostats.   The simulation

was done using DMol^3 package and all parameters and details are the same with the geometry optimization.

For all snapshot configurations extracted from the 2 ps trajectory, DFT calculations were performed using Gaussian 03 package. As we are interested in potential diradical character of the thermodynamic ensemble of pentacene and not of the minimum structure, the molecular coordinates were directly taken from the 2 ps AIMD trajectory without further DFT optimizations. Initially, we took configurations from the trajectory every 10 fs, and obtained their closed-shell singlet (CS), open-shell broken-symmetry singlet (BS), triplet (T) states through single-point calculations at the (U)B3LYP/6-31G(d,p) level of theory. To confirm the results of the B3LYP method, the CASSCF (10, 10) calculations were also performed to determine the orbital occupation numbers for the snapshot configurations possessing diradical character. All CASSCF calculations were preformed at a 6-31G(d) basis set level. By doing so, we got the ground state of each snapshot configuration (not the global minimum at potential energy surface of pentacene molecule) and the energetic criteria of diradical character appearing. In addition, we chose some typical short trajectories (two arbitrary time regions in the 2 ps trajectory) for more detailed analyses. To do this, we did conformational sampling every 1 fs in order to explore the inherent factors which dominate the appearance of diradical character of pentacene.

To clarify possible association of the snapshot configurations with diradical character with molecular vibrational modes, we optimized pentacene molecule at the B3LYP/6-31G(d,p) level with frequency analysis and further examined diradical character of its 102 distorted configurations according to the 102 vibrational modes. Each distorted configuration is generated by adding the shift vector coordinates (x, y, z) of each atom in a vibrational mode to the corresponding coordinates of that atom in standard orientation. For each vibrational mode-distorted configuration, the energies of three states (closed-shell singlet state (CS), open-shell broken-symmetry singlet state (OS or BS), and triplet state (T)) are calculated, together with other parameters such as HOMO and LUMO energies and their gaps, singlet-triplet state energy gaps, spin contamination $<S^2>$, vibrational frequencies and periods, and HOMO, LUMO, or SOMO, spin densities, and so on are given below (Table S12).

3. Relevant Data for Describing Diradical Character

Table S1. The numbers of electrons outside closed-shell bonding orbitals (BO), occupation numbers of HOMO and LUMO, and diradical percentages for configurations with diradical character calculated using the CASSCF(10,10)/6-31G(d) method.

Note that configuration at 0 fs corresponds to the static pentacene.

Simulation Time (fs)	Total occupancy outside BO	Occupation number of HOMO	Occupation number of LUMO	Diradical percentage (%)
0	0.343	1.882	0.121	12.1
50	0.488	1.853	0.152	15.2
120	0.465	1.861	0.144	14.4
140	0.510	1.837	0.167	16.7
160	0.538	1.778	0.225	22.5
210	0.495	1.846	0.158	15.8
280	0.440	1.850	0.153	15.3
300	0.516	1.785	0.218	21.8
390	0.599	1.716	0.287	28.7
410	0.486	1.848	0.156	15.6
430	0.493	1.838	0.167	16.7
500	0.527	1.794	0.208	20.8
610	0.484	1.856	0.149	14.9
650	0.502	1.813	0.190	19.0
700	0.473	1.855	0.149	14.9
720	0.460	1.840	0.164	16.4
740	0.452	1.848	0.155	15.5
760	0.430	1.863	0.141	14.1
810	0.480	1.858	0.147	14.7
830	0.527	1.780	0.222	22.2
900	0.525	1.793	0.210	21.0
920	0.489	1.849	0.156	15.6
990	0.473	1.814	0.189	18.9
1010	0.458	1.865	0.140	14.0
1160	0.472	1.860	0.145	14.5
1520	0.483	1.812	0.191	19.1
1580	0.472	1.854	0.151	15.1
1780	0.526	1.791	0.211	21.1
1800	0.500	1.806	0.197	19.7
1890	0.488	1.856	0.150	15.0
1960	0.492	1.790	0.213	21.3

Table S2. Spin contaminations for the open-shell BS singlet ($<S^2>$) and energy orders of 200 snapshot configurations extracted from a 2 ps trajectory one every 10 fs, calculated at the UB3LYP/6-31G(d,p) level (the original data for Figure 1 in the text)

Simulation Times (fs)	$<S^2>$	Energy Orders	Simulation Times (fs)	$<S^2>$	Energy Orders
0-40	0	$E_{(CS)} < E_{(T)}$	750	0	$E_{(CS)} < E_{(T)}$
50	0.10	$E_{(BS)} < E_{(CS)} < E_{(T)}$	760	0.04	$E_{(BS)} < E_{(CS)} < E_{(T)}$
60-110	0	$E_{(CS)} < E_{(T)}$	770-800	0	$E_{(CS)} < E_{(T)}$
120	0.09	$E_{(BS)} < E_{(CS)} < E_{(T)}$	810	0.09	$E_{(BS)} < E_{(CS)} < E_{(T)}$
130	0	$E_{(CS)} < E_{(T)}$	820	0	$E_{(CS)} < E_{(T)}$
140	0.35	$E_{(BS)} < E_{(CS)} < E_{(T)}$	830	0.02	$E_{(BS)} < E_{(CS)} < E_{(T)}$
150	0	$E_{(CS)} < E_{(T)}$	840-890	0	$E_{(CS)} < E_{(T)}$
160	0.10	$E_{(BS)} < E_{(CS)} < E_{(T)}$	900	0.2	$E_{(BS)} < E_{(CS)} < E_{(T)}$
170-200	0	$E_{(CS)} < E_{(T)}$	910	0	$E_{(CS)} < E_{(T)}$
210	0.28	$E_{(BS)} < E_{(CS)} < E_{(T)}$	920	0.14	$E_{(BS)} < E_{(CS)} < E_{(T)}$
220-270	0	$E_{(CS)} < E_{(T)}$	930-980	0	$E_{(CS)} < E_{(T)}$
280	0.10	$E_{(BS)} < E_{(CS)} < E_{(T)}$	990	0.01	$E_{(BS)} < E_{(CS)} < E_{(T)}$
290	0	$E_{(CS)} < E_{(T)}$	1000	0	$E_{(CS)} < E_{(T)}$
300	0.07	$E_{(BS)} < E_{(CS)} < E_{(T)}$	1010	0.02	$E_{(BS)} < E_{(CS)} < E_{(T)}$
310-380	0	$E_{(CS)} < E_{(T)}$	1020-1150	0	$E_{(CS)} < E_{(T)}$
390	0.08	$E_{(BS)} < E_{(CS)} < E_{(T)}$	1160	0.11	$E_{(BS)} < E_{(CS)} < E_{(T)}$
400	0	$E_{(CS)} < E_{(T)}$	1170-1510	0	$E_{(CS)} < E_{(T)}$
410	0.07	$E_{(BS)} < E_{(CS)} < E_{(T)}$	1520	0.09	$E_{(BS)} < E_{(CS)} < E_{(T)}$
420	0	$E_{(CS)} < E_{(T)}$	1530-1570	0	$E_{(CS)} < E_{(T)}$
430	0.18	$E_{(BS)} < E_{(CS)} < E_{(T)}$	1580	0.13	$E_{(BS)} < E_{(CS)} < E_{(T)}$
440-490	0	$E_{(CS)} < E_{(T)}$	1590-1770	0	$E_{(CS)} < E_{(T)}$
500	0.04	$E_{(BS)} < E_{(CS)} < E_{(T)}$	1780	0.21	$E_{(BS)} < E_{(CS)} < E_{(T)}$
510-600	0	$E_{(CS)} < E_{(T)}$	1790	0	$E_{(CS)} < E_{(T)}$
610	0.12	$E_{(BS)} < E_{(CS)} < E_{(T)}$	1800	0.08	$E_{(BS)} < E_{(CS)} < E_{(T)}$
620-640	0	$E_{(CS)} < E_{(T)}$	1810-1880	0	$E_{(CS)} < E_{(T)}$
650	0.23	$E_{(BS)} < E_{(CS)} < E_{(T)}$	1890	0.13	$E_{(BS)} < E_{(CS)} < E_{(T)}$
660-690	0	$E_{(CS)} < E_{(T)}$	1900-1950	0	$E_{(CS)} < E_{(T)}$
700	0.18	$E_{(BS)} < E_{(CS)} < E_{(T)}$	1960	0.09	$E_{(BS)} < E_{(CS)} < E_{(T)}$
710	0	$E_{(CS)} < E_{(T)}$	1970-2000	0	$E_{(CS)} < E_{(T)}$
720	0.14	$E_{(BS)} < E_{(CS)} < E_{(T)}$			
730	0	$E_{(CS)} < E_{(T)}$			
740	0.10	$E_{(BS)} < E_{(CS)} < E_{(T)}$			

Table S3. Spin contaminations for the open-shell BS singlet ($<S^2>$) of snapshot configurations extracted one every 1 fs from two time ranges (640-840 fs and 1700-1900 fs) in a 2 ps trajectory, calculated at the UB3LYP/6-31G(d,p) level (the original data for Figure 6)

Simulation Times (fs)	$<S^2>$	Simulation Times (fs)	$<S^2>$	Simulation Times (fs)	$<S^2>$
640-647	0.0	743	0.201	1700-1715	0.0
648	0.051	744	0.154	1716	0.002
649	0.157	745	0.079	1717-1775	0.0
650	0.230	746-759	0.0	1776	0.028
651	0.285	760	0.037	1777	0.107
652	0.312	761	0.141	1778	0.157
653	0.316	762	0.200	1779	0.189
654	0.294	763	0.243	1780	0.207
655	0.245	764	0.266	1781	0.203
656	0.170	765	0.257	1782	0.184
657	0.060	766	0.219	1783	0.148
658-672	0.0	767	0.151	1784	0.074
673	0.098	768	0.037	1785-1798	0.0
674	0.154	769-781	0.0	1799	0.041
675	0.181	782	0.019	1800	0.081
676	0.168	783	0.09952	1801	0.112
677	0.131	784	0.161	1802	0.109
678	0.068	785	0.210	1803	0.107
679-695	0.0	786	0.219	1804	0.083
696	0.105	787	0.205	1805	0.031
697	0.187	788	0.166	1806-1823	0.0
698	0.227	789	0.087	1824	0.004
699	0.224	790-805	0.0	1825	0.066
700	0.179	806	0.022	1826	0.099
701	0.092	807	0.093	1827	0.109
702-718	0.0	808	0.118	1828	0.087
719	0.065	809	0.119	1829	0.042
720	0.140	810	0.095	1830-1888	0.0
721	0.172	811	0.028	1889	0.064
722	0.160	812-829	0.0	1890	0.128
723	0.113	830	0.016	1891	0.162
724	0.034	831	0.047	1892	0.172
725-739	0.0	832	0.044	1893	0.153
740	0.104	833	0.016	1894	0.113
741	0.173	834-840	0.0	1895	0.056
742	0.210			1896-1900	0.0

Table S4. Calculated energies (in au), $\langle S^2 \rangle$ values, and intramolecular magnetic exchange coupling constants (J in cm^{-1}) at the UB3LYP/6-31G(d,p) level for a part of snapshot configurations with diradical character

Simulation Times (fs)	$E_{(T)}$ ($\langle S^2 \rangle$)	$E_{(BS)}$ ($\langle S^2 \rangle$)	J (cm^{-1})
50	-846.73298754 (2.030)	-846.76046199 (0.103)	-3129.3
120	-846.75739962 (2.029)	-846.78513529 (0.069)	-3106.5
140	-846.73146102 (2.032)	-846.75396142 (0.353)	-2940.7
160	-846.71941541 (2.030)	-846.74642417 (0.099)	-3069.8
210	-846.73603171 (2.032)	-846.75939775 (0.284)	-2933.9
280	-846.72061700 (2.030)	-846.74750753 (0.104)	-3063.1
300	-846.73972245 (2.029)	-846.76777767 (0.071)	-3145.4
390	-846.73832425 (2.032)	-846.76620531 (0.080)	-3136.0
410	-846.73721394 (2.029)	-846.76513962 (0.070)	-3129.7
430	-846.72885487 (2.029)	-846.75401411 (0.185)	-2994.7
500	-846.73501782 (2.030)	-846.76355127 (0.037)	-3142.3
610	-846.75423117 (2.030)	-846.78098432 (0.119)	-3071.5
650	-846.73149004 (2.033)	-846.75605386 (0.230)	-2990.1
700	-846.73853302 (2.031)	-846.76393470 (0.179)	-3010.1
720	-846.74611654 (2.030)	-846.77237359 (0.140)	-3049.9
740	-846.73492725 (2.031)	-846.76240200 (0.104)	-3128.7
760	-846.73949395 (2.029)	-846.76812018 (0.037)	-3153.4
810	-846.75105538 (2.029)	-846.77841593 (0.095)	-3104.6
830	-846.74093878 (2.033)	-846.76938721 (0.016)	-3096.2
900	-846.74799236 (2.030)	-846.77339585 (0.199)	-3045.6
920	-846.75816968 (2.031)	-846.78436928 (0.142)	-3043.7
990	-846.74477200 (2.029)	-846.77316252 (0.009)	-3083.9
1010	-846.73582729 (2.032)	-846.76458943 (0.019)	-3137.0
1160	-846.73329487 (2.031)	-846.75985990 (0.111)	-3036.8
1520	-846.74330420 (2.030)	-846.77052005 (0.086)	-3072.9
1580	-846.72978714 (2.029)	-846.75593503 (0.129)	-3021.2
1780	-846.72442327 (2.036)	-846.74992843 (0.207)	-3059.7
1800	-846.72861481 (2.027)	-846.75591497 (0.081)	-3077.7
1890	-846.73754610 (2.029)	-846.76398393 (0.128)	-3051.5
1960	-846.74311754 (2.032)	-846.77063084 (0.087)	-3104.7

Note: We use a simple broken-symmetry (BS) formalism which was developed by Yamaguchi *et al*. (Yamaguchi, K.; Takahara, Y.; Fueno, T.; Nasu, K. *Jpn. J. Appl. Phys.* **1987**, *26*, L1362. Yamaguchi, K.; Jensen, F.; Dorigo, A.; Houk, K. N. *Chem. Phys. Lett.* **1988**, *149*, 537) and regarded as the most appropriate one for estimating magnetic exchange coupling interaction in diradicals to estimate the J value. The formula is given as $J = \dfrac{E_{BS} - E_T}{\langle S^2 \rangle_T - \langle S^2 \rangle_{BS}}$, where E_{BS} and E_T refer to the energies of unrestricted open-shell BS singlet and triplet states, while $\langle S^2 \rangle_{BS}$ and $\langle S^2 \rangle_T$ are the corresponding average spin square $\langle S^2 \rangle$ values, respectively.

4. Variations of Molecular Lengths in Time Evolution

Table S5. Molecular lengths (Å) of snapshot configurations extracted from the trajectory one every 1 fs in the time range of 760-833 fs

Simulation Time (fs)	Molecular lengths (Å)	Simulation Time (fs)	Molecular lengths (Å)	Simulation Time (fs)	Molecular lengths (Å)
760	12.23	769	12.25	812	12.13
761	12.23	770	12.25	813	12.12
762	12.24	771	12.24	814	12.12
763	12.24	772	12.24	815	12.11
764	12.25	773	12.24	816	12.10
765	12.25	774	12.24	817	12.10
766	12.25	775	12.23	818	12.09
767	12.25	776	12.23	819	12.08
768	12.25	777	12.23	820	12.08
760-768	**12.24**	778	12.22	821	12.07
782	12.21	779	12.22	822	12.07
783	12.20	780	12.22	823	12.07
784	12.20	781	12.21	824	12.07
785	12.19	**769-781**	**12.23**	825	12.07
786	12.19	790	12.16	826	12.07
787	12.18	791	12.15	827	12.08
788	12.17	792	12.14	828	12.08
789	12.16	793	12.14	829	12.08
782-789	**12.19**	794	12.13	**812-829**	**12.09**
806	12.16	795	12.13		
807	12.16	796	12.13		
808	12.15	797	12.13		
809	12.15	798	12.13		
810	12.14	799	12.13		
811	12.14	800	12.14		
806-811	**12.15**	801	12.14		
830	12.08	802	12.14		
831	12.08	803	12.15		
832	12.08	804	12.15		
833	12.08	805	12.15		
830-833	**12.08**	**790-805**	**12.14**		
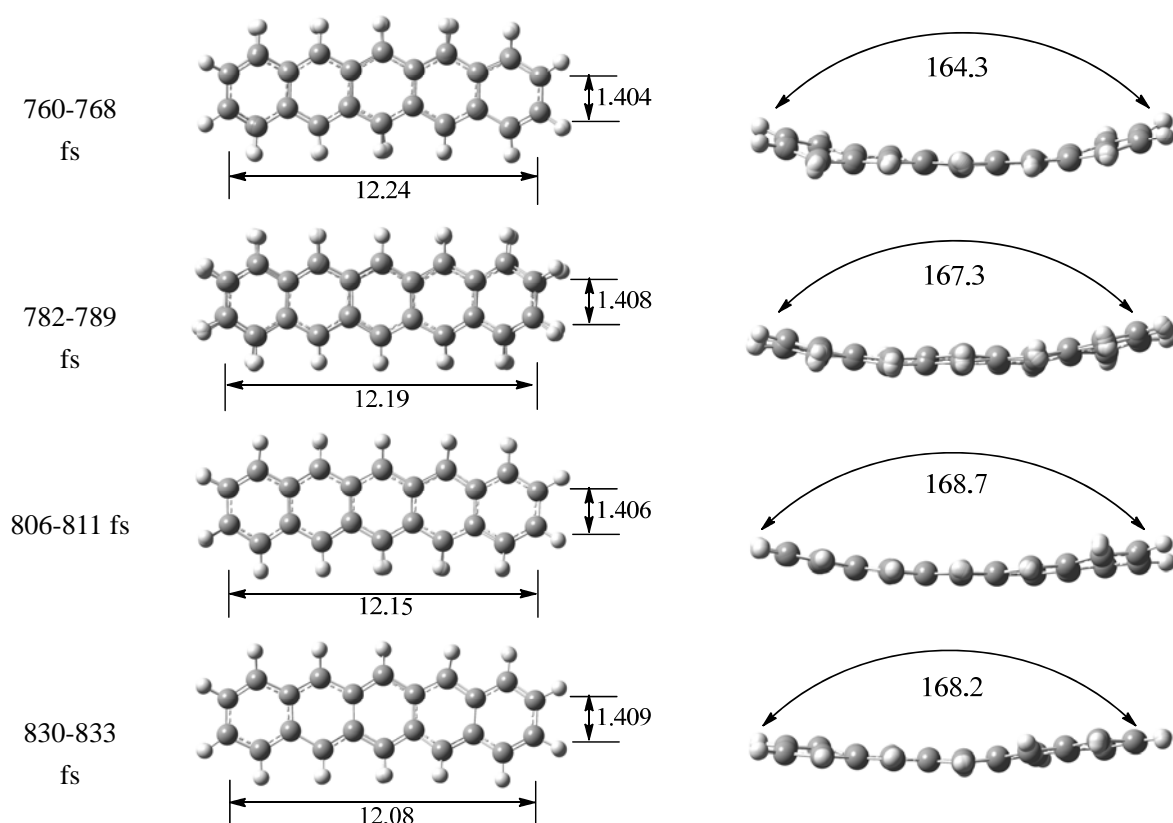
Figure S1. Geometry evolution in four typical time ranges in the trajectory and main geometrical parameters: molecular lengths measured by the marked C…C distance, C-C bond lengths of the most outer ones, and bending angles.
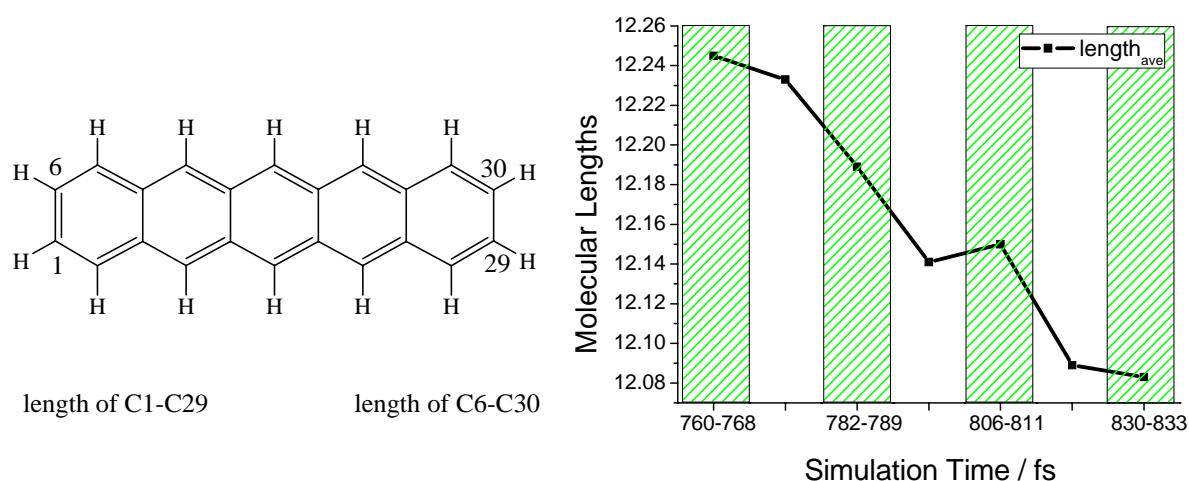
Figure S2. Average molecular lengths (Å) in different time ranges along with the simulation time according to data in Table S5 and Figure S1. The sparse green-line filled areas denote the time ranges in which the diradical character appears. This figure shows no correlation between the diradical character and the average molecular length.
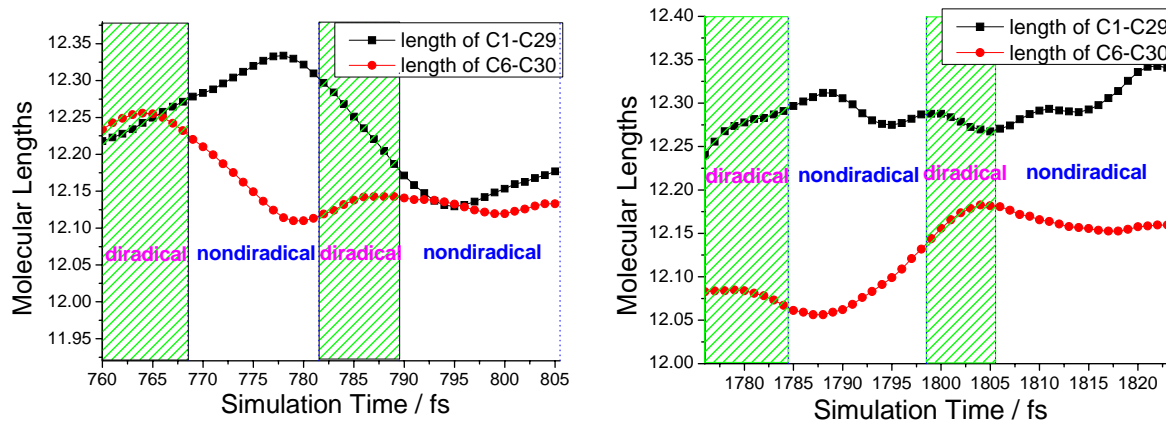
Figure S3. Molecular length evolution (Å) of instantaneous configurations extracted every 1 fs from 760 fs to 805 fs (**Left**) and from 1776 fs to 1823 fs (**Right**), respectively. The sparse green-line filled areas denote the time ranges in which the diradical character appears. There is no correlation between the diradical character and molecular length.

5. Variations of the Cross-Linking C-C Bonds in Time Evolution

We monitor the changes of six cross-linking C-C bonds (that is, C1-C6, C3-C4, C9-C8, C12-C13, C16-C17, and C29-C30) along the evolution time, and those for the average, longest, and shortest C-C bonds are give in Table S6. The changes of them and all six C-C bonds in two time ranges (760-805 fs, 1776-1823 fs) are displayed in Figure S4.
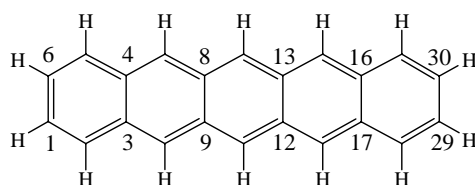
Table S6. Cross-linking C-C bonds (Å) of snapshot configurations extracted from the trajectory one every 1 fs in the time range of 760-833 fs. Note that C-C$_{ave}$ are the average values of six cross-linking C-C bonds of each configuration, while C-C$_{shortest}$ and C-C$_{longest}$ are the average values of the shortest and the longest C-C bonds, respectively. Besides, values in bold of the 2nd, 3rd, 4th, 6th, 7th and 8th columns are all average ones of the corresponding time ranges (1st and 5th columns).

Simulation Times (fs)	C-C$_{ave}$ (Å)	C-C$_{shortest}$ (Å)	C-C$_{longest}$ (Å)	Simulation Times (fs)	C-C$_{ave}$ (Å)	C-C$_{shortest}$ (Å)	C-C$_{longest}$ (Å)
760	1.432	1.395	1.475	769	1.449	1.428	1.497
761	1.426	1.394	1.467	770	1.457	1.431	1.508
762	1.423	1.395	1.460	771	1.464	1.435	1.516
763	1.421	1.399	1.451	772	1.471	1.441	1.522
764	1.421	1.405	1.443	773	1.478	1.446	1.524
765	1.423	1.407	1.436	774	1.482	1.451	1.523
766	1.428	1.408	1.449	775	1.485	1.446	1.519
767	1.433	1.411	1.466	776	1.486	1.452	1.528
768	1.441	1.421	1.481	777	1.485	1.447	1.536
760-768	**1.428**	**1.404**	**1.459**	778	1.482	1.441	1.540
782	1.457	1.413	1.517	779	1.477	1.435	1.539
783	1.451	1.410	1.506	780	1.471	1.428	1.535
784	1.445	1.407	1.493	781	1.464	1.421	1.527
785	1.439	1.405	1.476	**769-781**	**1.473**	**1.439**	**1.524**
786	1.436	1.405	1.462	790	1.437	1.408	1.473
787	1.434	1.406	1.450	791	1.439	1.407	1.484
788	1.433	1.409	1.448	792	1.443	1.409	1.495
789	1.434	1.410	1.460	793	1.448	1.410	1.504
782-789	**1.441**	**1.408**	**1.477**	794	1.454	1.413	1.511
806	1.437	1.401	1.460	795	1.458	1.416	1.515
807	1.433	1.397	1.452	796	1.462	1.419	1.514
808	1.432	1.398	1.446	797	1.464	1.421	1.510
809	1.431	1.403	1.445	798	1.466	1.423	1.503
810	1.432	1.412	1.447	799	1.466	1.425	1.500
811	1.435	1.423	1.452	800	1.463	1.425	1.499
806-811	**1.433**	**1.406**	**1.450**	801	1.460	1.425	1.496
830	1.437	1.400	1.479	802	1.456	1.427	1.491
831	1.435	1.405	1.468	803	1.451	1.428	1.484
832	1.435	1.411	1.458	804	1.446	1.421	1.477
833	1.436	1.418	1.452	805	1.441	1.409	1.468
830-833	**1.436**	**1.409**	**1.464**	**790-805**	**1.453**	**1.418**	**1.495**
				812	1.438	1.425	1.456
				813	1.443	1.428	1.461

814	1.448	1.434	1.470
815	1.453	1.436	1.482
816	1.458	1.437	1.492
817	1.463	1.437	1.503
818	1.467	1.436	1.512
819	1.470	1.435	1.516
820	1.471	1.431	1.519
821	1.471	1.426	1.518
822	1.468	1.418	1.520
823	1.466	1.411	1.524
824	1.462	1.407	1.526
825	1.457	1.403	1.524
826	1.452	1.399	1.519
827	1.447	1.397	1.512
828	1.443	1.397	1.504
829	1.440	1.398	1.494
812-829	**1.457**	**1.420**	**1.503**
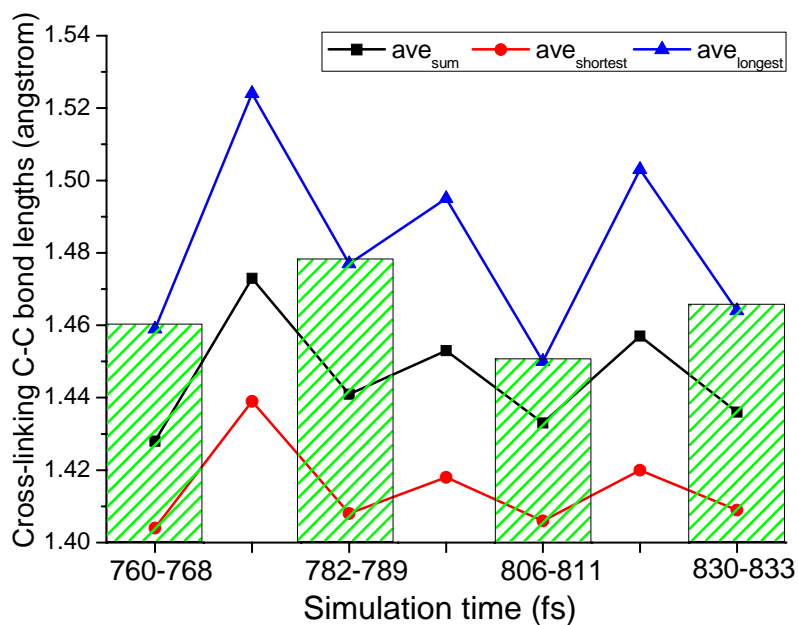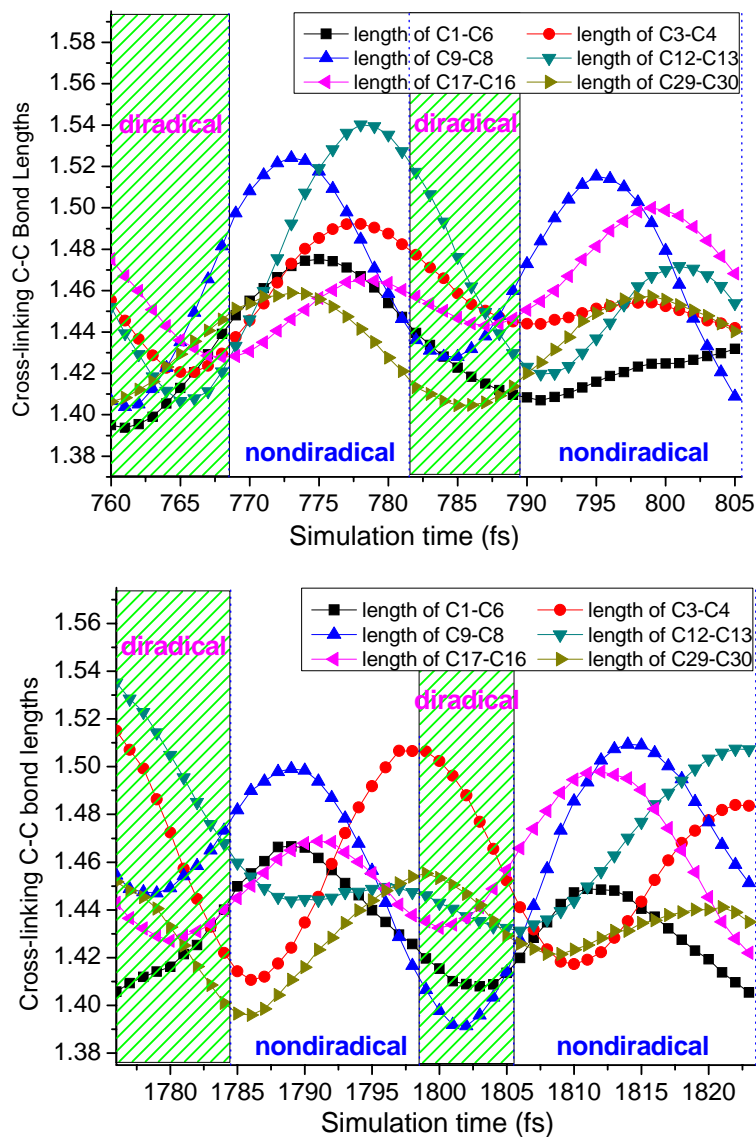
Figure S4. (**The *first***) Average cross-linking C-C bond lengths (Table S6, Å) in different time ranges of the simulation trajectory, where ave_{sum}, $ave_{shortest}$ and $ave_{longest}$ denote the average ones over all six, the shortest, and the longest cross-linking C-C bonds, respectively. The sparse green-line filled areas denote the time ranges in which the diradical character appears. The right is the pentacene structure with the corresponding atomic numbering. Time evolution of the cross-linking C-C bond lengths (Å) of instantaneous configurations extracted every 1 fs in 760-805 fs (**the *second***) and in 1776-1823 fs (**the *third***) from the simulation trajectory, respectively. The sparse green-line filled areas denote the time ranges in which the diradical character appears.

6. Molecular Bending Effect

To check if there is a relationship between molecular bending and diradical character appearing for pentacene in time evolution, we measure the molecular bending angle according to the following definition (chart).   That is, the bending angle is defined by $\angle 123$ marked in the chart.   Relevant bending angles along the time are given in Table S7 and also displayed in Figure S5 and S6.   Together with the calculated possible diradical character, these data do not present any relationship with the diradical character of snapshot configurations of pentacene. In other words, the molecular bending is not a driving factor for diradical character appearing for some snapshot configurations of pentacene.
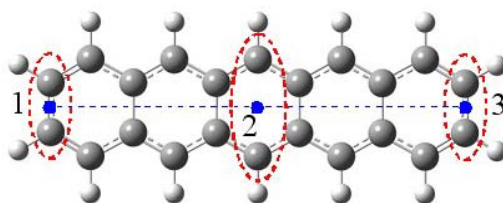
To further clarify this issue, we also calculate the electronic properties of bent pentacene model extracted from the corresponding single-wall carbon nanotube (SWCNT).   Each extracted configuration is saturated by hydrogen atoms for the cutting bonds, forming the corresponding bent model pentacene configuration with a bending angle ($\angle 123$).   Then, two cases are considered: **i)** the configuration is directly calculated for examining its diradical character; **ii)** by fixing its C1-C29 and C6-C30 distances the configuration is further optimized partially and then calculated for examining its diradical character.   Results indicate that for the case **i)** all model configurations extracted directly from SWCNTs exhibit diradical character, as shown in Table S8, but for the case **ii)** the diradical character for all configurations disappears, as shown in Table S9. Comparison between these two cases indicates that a bent pentacene (relaxed) does not have diradical character unless its backbone is tensioned (unrelaxed).

Thus, we can conclude that just a bending does not trigger pentacene a diradical character, and thus observed diradical character of pentacene in time evolution must be attributed to other factors (e.g. other geometrical distortions).

Table S7. Bending Angles (°) of Snapshot Configurations Extracted from the Trajectory One Every 1 fs in the Time Range of 760-833 fs

Simulation Time (fs)	Bending angles (°)	Simulation Time (fs)	Bending angles (°)	Simulation Time (fs)	Bending angles (°)
760	164.1	769	164.8	812	168.8
761	164.1	770	164.9	813	168.8
762	164.2	771	165.1	814	168.8
763	164.2	772	165.2	815	168.8
764	164.3	773	165.3	816	168.8
765	164.4	774	165.5	817	168.8
766	164.4	775	165.7	818	168.8
767	164.6	776	165.8	819	168.8
768	164.7	777	166.0	820	168.7
760-768	**164.3**	778	166.2	821	168.7
782	166.8	779	166.4	822	168.7
783	167.0	780	166.5	823	168.7
784	167.1	781	166.7	824	168.6
785	167.2	**769-781**	**165.7**	825	168.6
786	167.4	790	167.8	826	168.5
787	167.5	791	167.9	827	168.5
788	167.6	792	168.0	828	168.4
789	167.7	793	168.1	829	168.4
782-789	**167.3**	794	168.1	**812-829**	**168.7**
806	168.6	795	168.2		
807	168.7	796	168.3		
808	168.7	797	168.3		
809	168.7	798	168.4		
810	168.8	799	168.4		
811	168.8	800	168.4		
806-811	**168.7**	801	168.5		
830	168.3	802	168.5		
831	168.3	803	168.6		
832	168.2	804	168.6		
833	168.2	805	168.6		
830-833	**168.2**	**790-805**	**168.3**		

Note: the values in bold are average bending angles of the corresponding time ranges.
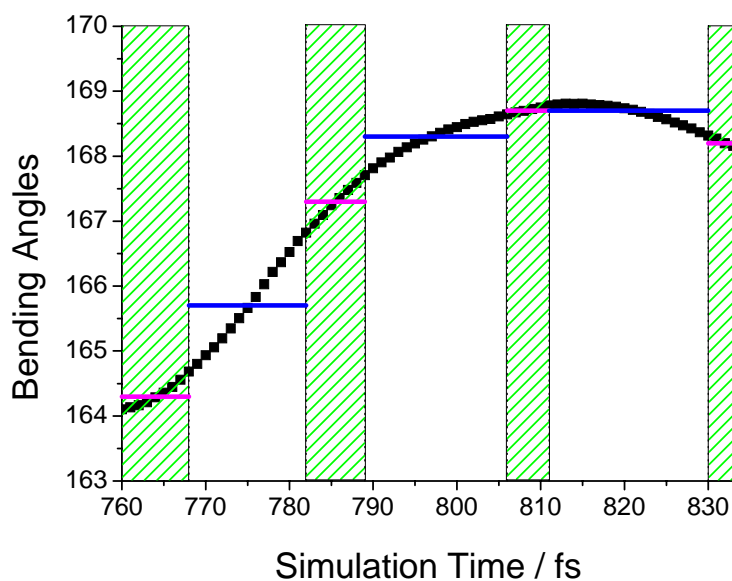
Figure S5. The bending angles (degree) of configurations extracted every 1 from the simulation trajectory in the range of 760-833 fs, and the pink and blue bars correspond to the average bending angles (degree) of different time ranges with and without diradical character, respectively. Also, the time ranges with diradical character are marked by sparse green lines.
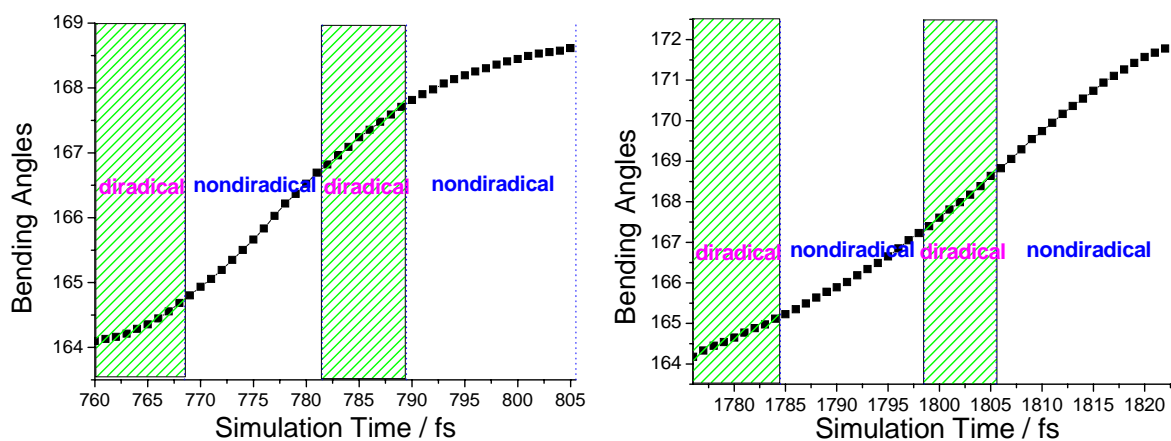
Figure S6. The bending angles (degree) of configurations extracted every 1 fs from the simulation trajectory in the range of 760-805 fs (**Left**) and in 1776-1823 fs (**Right**), respectively. The sparse green-line filled areas denote the time ranges in which the diradical character appears.

Table S8. Bending Angles (°) of Configurations Extracted Directly from Different SWCNTs (Single-Point Calculations). (**Note:** Blue Dots Are the Corresponding Centroids of Carbon Atoms in the Corresponding Red Circles, and the Bending Angle Is Referred to the Angle between Three Centroids in One Configuration)
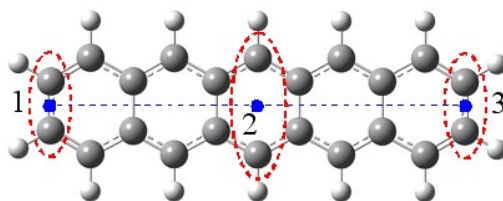
Bending Angles (°)	$\langle S^2 \rangle$	Bending Angles (°)	$\langle S^2 \rangle$
168.1 (SWCNT76)	0.35	158.6 (SWCNT42)	0.36
167.8 (SWCNT74)	0.35	157.5 (SWCNT40)	0.36
167.5 (SWCNT72)	0.36	156.3 (SWCNT38)	0.36
167.1 (SWCNT70)	0.35	155.0 (SWCNT36)	0.36
166.8 (SWCNT68)	0.36	153.5 (SWCNT34)	0.36
166.4 (SWCNT66)	0.36	151.9 (SWCNT32)	0.37
166.0 (SWCNT64)	0.36	150.0 (SWCNT30)	0.37
165.5 (SWCNT62)	0.36	147.9 (SWCNT28)	0.37
165.0 (SWCNT60)	0.35	145.4 (SWCNT26)	0.38
164.5 (SWCNT58)	0.36	142.5 (SWCNT24)	0.37
164.0 (SWCNT56)	0.36	139.1 (SWCNT22)	0.39
163.3 (SWCNT54)	0.37	135.0 (SWCNT20)	0.39
162.7 (SWCNT52)	0.36	130.0 (SWCNT18)	0.40
162.0 (SWCNT50)	0.35	123.7 (SWCNT16)	0.41
161.3 (SWCNT48)	0.36	115.7 (SWCNT14)	0.43
160.4 (SWCNT46)	0.36	105.0 (SWCNT12)	0.45
159.6 (SWCNT44)	0.36		

Note: for each structure with the given bending angle, all other geometrical parameters are not relaxed.

Table S9. Bending angles (°) of the configurations extracted from different SWCNTs with partially optimized parameters (lengths of C1-C29 and C6-C30 are fixed and other geometrical parameters are optimized for each configuration extracted from the corresponding SWCNT). Note that all these partially optimized configurations do not have diradical character.
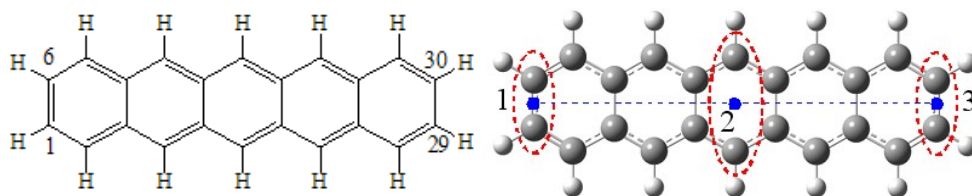
Pentacene structures extracted from different SWCNTs	Bending angles (°)	$<S^2>$
SWCNT76-Pentacene	168.1	0
SWCNT64-Pentacene	166.0	0
SWCNT56-Pentacene	164.0	0
SWCNT50-Pentacene	162.0	0
SWCNT44-Pentacene	159.6	0
SWCNT22-Pentacene	139.1	0
SWCNT18-Pentacene	130.0	0
SWCNT16-Pentacene	123.7	0
SWCNT14-Pentacene	115.7	0
SWCNT12-Pentacene	105.0	0

7. Hydrogen Swing Effect

To clarify if the pure hydrogen swing motion can trigger the diradical character of pentacene molecule, we examine the effect of hydrogen swing on electronic properties. That is, we calculate the BS states of distorted pentacene due to the hydrogen swing by fixing the pentacene C backbone, keeping a plane, and only swinging a part of hydrogen atoms as mentioned in Table S10. In this examination, no in-plane (molecular plane) swing of any hydrogen atoms are considered, and only inward and outward motions (deviating from the

pentacene molecular plane) of a part of hydrogen atoms are considered. All of the distorted configurations considered here are classified as three situations (Table S10). Results indicate that all these distorted configurations do not have diradical character. That is, examinations suggest that no matter hydrogen stretching motion or hydrogen in-plane and out-of-plane swing motions do not trigger potential diradical character. Any motions of hydrogen atoms are not the driving factor of the diradical character appearing of pentacene.

The swing angle is defined as an angle of H-C(linked)-C(para position) in the same benzene ring, that is, the obtuse angle between the H-C bond and the molecular plane.
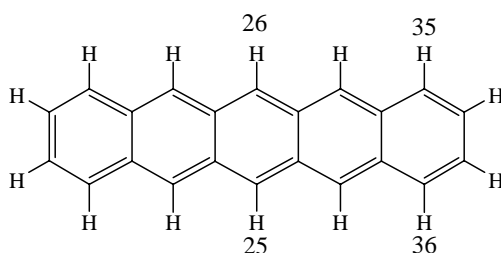
Table S10. Swing angles (°) of the distorted configurations by swinging the marked hydrogen atoms inward and outward and keeping all other atoms (C and H) in a plane (molecular plane)
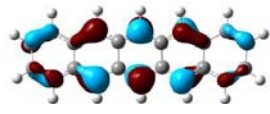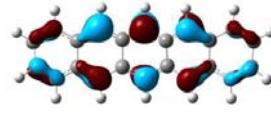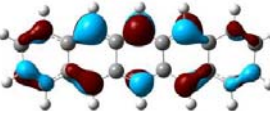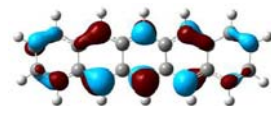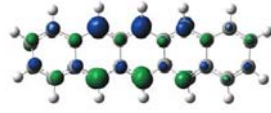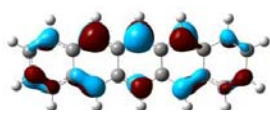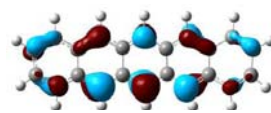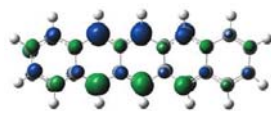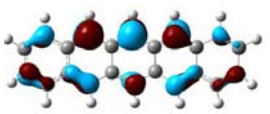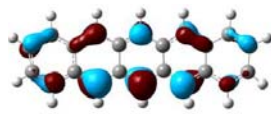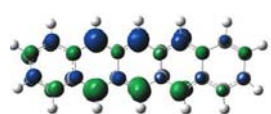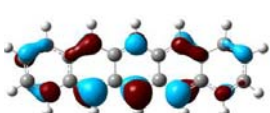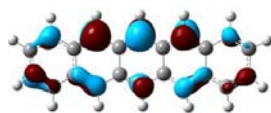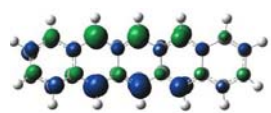
Situation 1	H35	H36	H26	H25	Other H atoms
$H35_{inward}H36_{inward}$	175.2	175.2	180.0	180.0	180.0
$H35_{inward}H36_{inward}$	175.7	173.9	180.0	180.0	180.0
$H35_{inward}H36_{inward}$	176.3	171.4	180.0	180.0	180.0
$H35_{inward}H36_{inward}$	172.5	178.4	180.0	180.0	180.0
$H35_{outward}H36_{inward}$	175.2	175.2	180.0	180.0	180.0
$H35_{outward}H36_{inward}$	175.7	173.9	180.0	180.0	180.0
$H35_{outward}H36_{inward}$	176.3	171.4	180.0	180.0	180.0
$H35_{outward}H36_{inward}$	172.5	178.4	180.0	180.0	180.0
Situation 2	**H35**	**H36**	**H26**	**H25**	**Other H atoms**
$H26_{inward}H25_{inward}$	180.0	180.0	175.2	175.2	180.0
$H26_{inward}H25_{inward}$	180.0	180.0	175.7	173.9	180.0
$H26_{inward}H25_{inward}$	180.0	180.0	176.3	171.4	180.0
$H26_{inward}H25_{inward}$	180.0	180.0	172.5	178.4	180.0
$H26_{outward}H25_{inward}$	180.0	180.0	175.2	175.2	180.0
$H26_{outward}H25_{inward}$	180.0	180.0	175.7	173.9	180.0
$H26_{outward}H25_{inward}$	180.0	180.0	176.3	171.4	180.0
$H26_{outward}H25_{inward}$	180.0	180.0	172.5	178.4	180.0
Situation 3	**H35**	**H36**	**H26**	**H25**	**Other H atoms**
$H26_{outward}H25_{inward}H35_{inward}H36_{outward}$	175.2	175.2	175.2	175.2	180.0
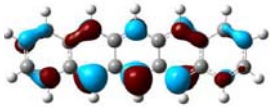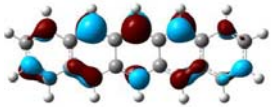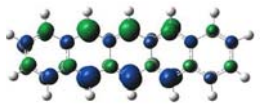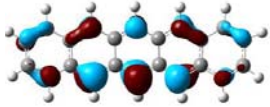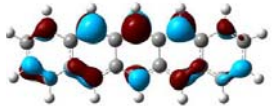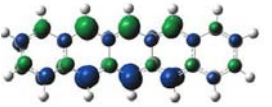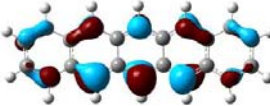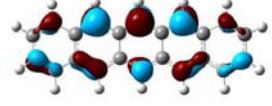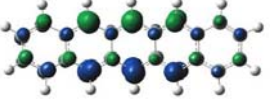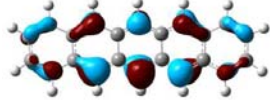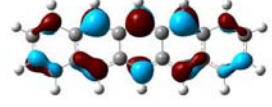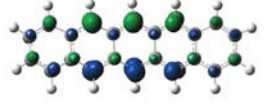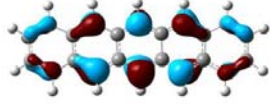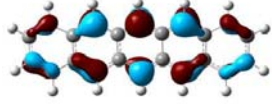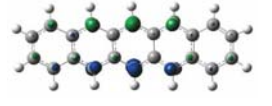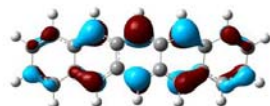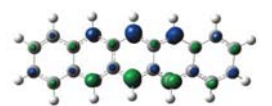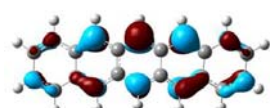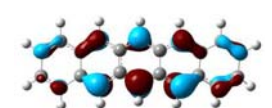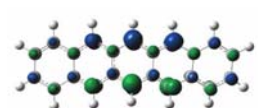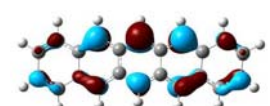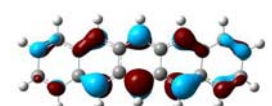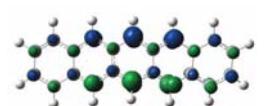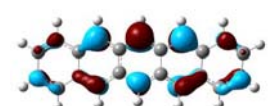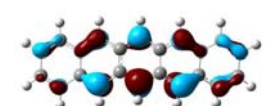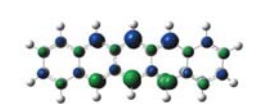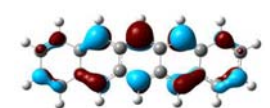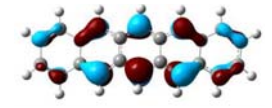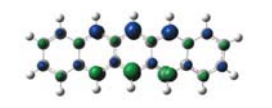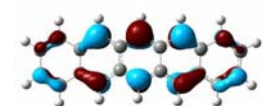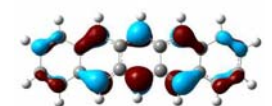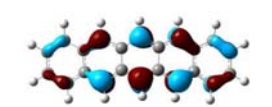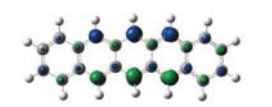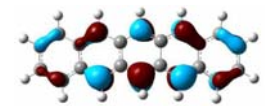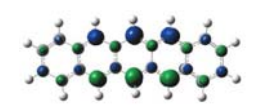
H26$_{inward}$H25$_{inward}$H35$_{inward}$H36$_{inward}$	176.2	171.4	172.6	178.4	180.0
H26$_{outward}$H25$_{inward}$H35$_{outward}$H36$_{inward}$	176.2	171.4	178.4	172.6	180.0
H26$_{inward}$H25$_{inward}$H35$_{outward}$H36$_{outward}$	171.4	176.2	172.6	178.4	180.0
H26$_{outward}$H25$_{outward}$H35$_{inward}$H36$_{inward}$	171.4	176.2	178.4	172.6	180.0
H26$_{inward}$H25$_{inward}$H35$_{inward}$H36$_{outward}$	170.0	170.0	170.0	170.0	180.0
H26$_{inward}$H25$_{outward}$H35$_{inward}$H36$_{inward}$	165.0	165.0	165.0	165.0	180.0
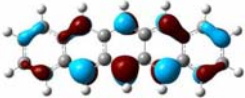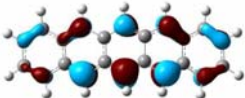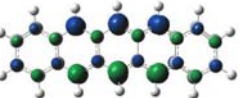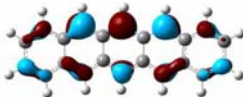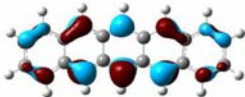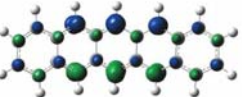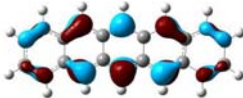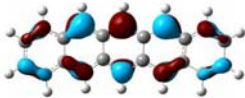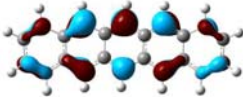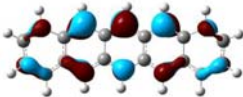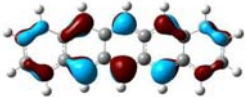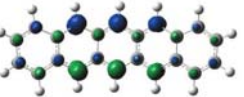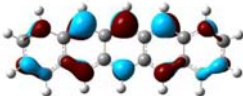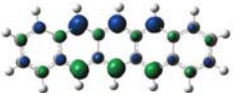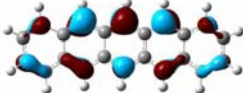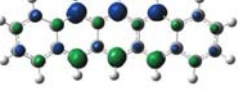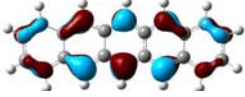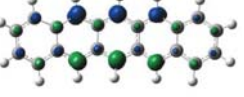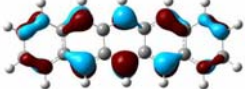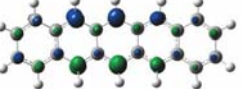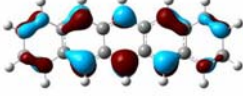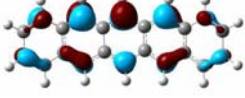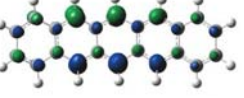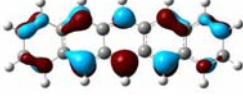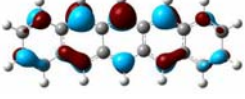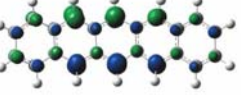
Note: the bending angle refers to the obtuse angle deviated (inward and outward) from the molecular plane for the marked atoms, e. g. $\angle HC_1C_2$ where the C_1 is the H-linked C, and the C_2 is the para-position C of C_1 in the same six-membered ring.
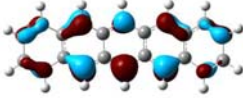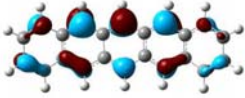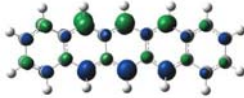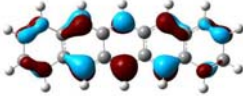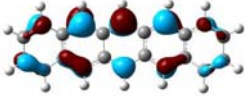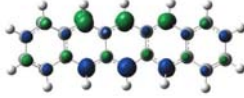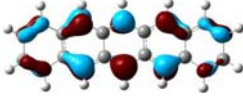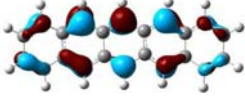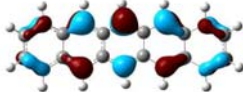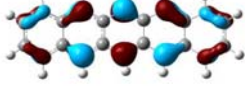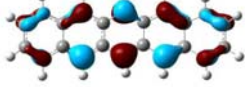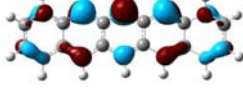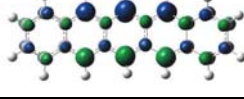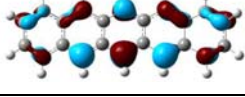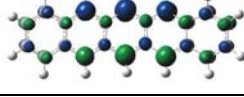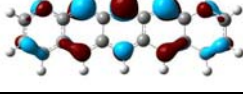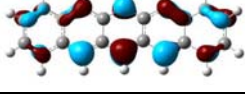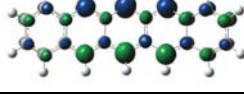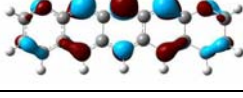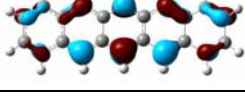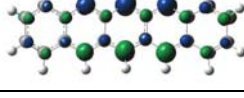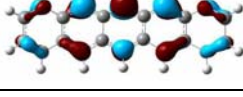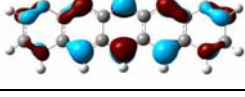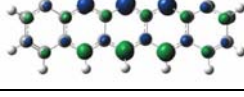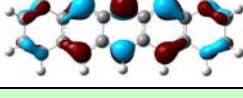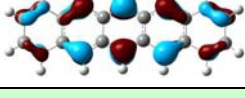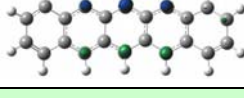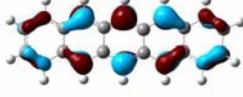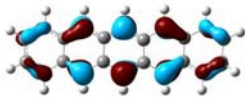
8. Singly Occupied Molecular Orbitals and Spin Density Distributions of Some Snapshot Configurations with Diradical Character Extracted from the AIMD Simulation Trajectory
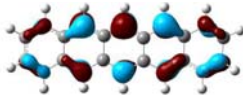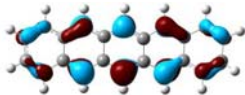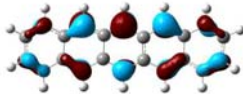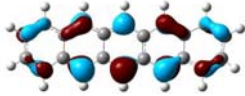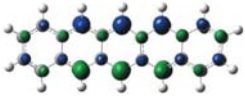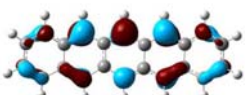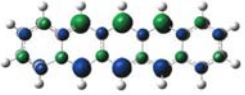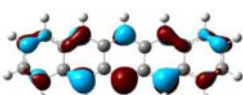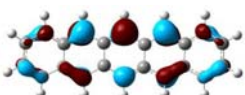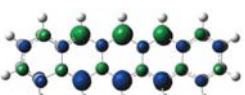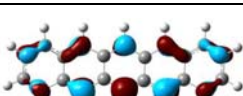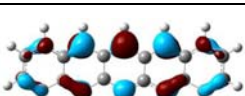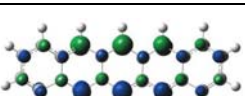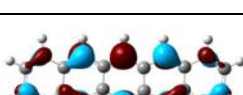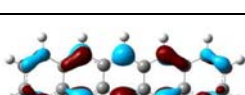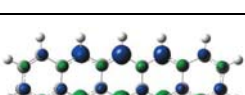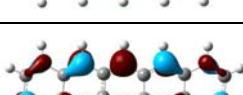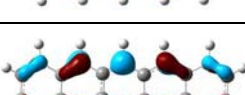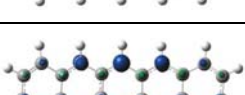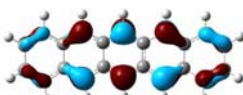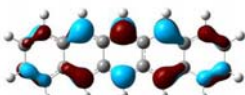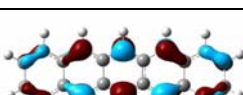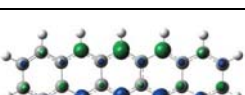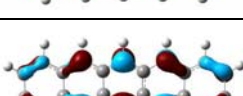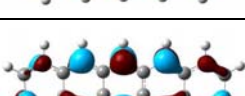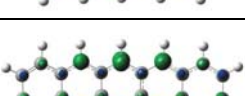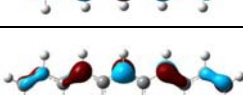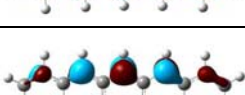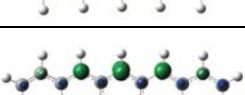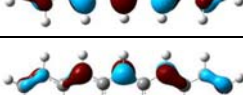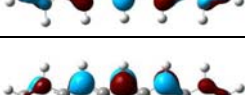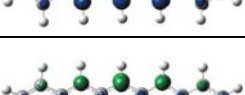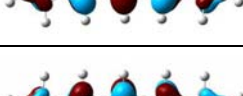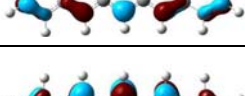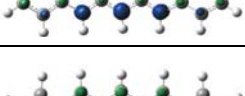
Table S11. Singly occupied molecular orbitals (SOMO, isovalue=0.04) and spin density distributions (isovalue=0.004) of the open-shell broken-symmetry (BS) singlet state for various instantaneous diradical configurations extracted from the AIMD simulation trajectory. **Note** that the isovalue values of spin density maps of the BS states for configurations at 1716 and 1824 fs are 0.0004
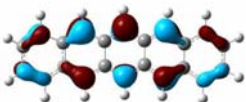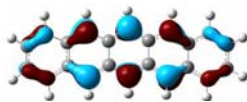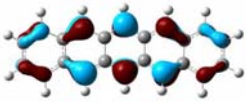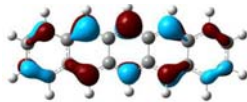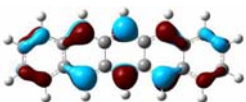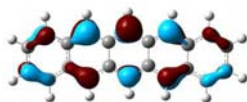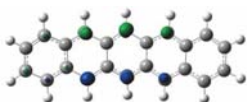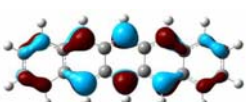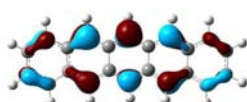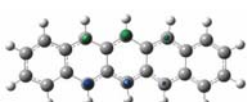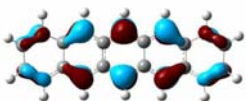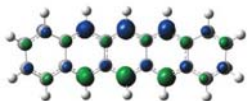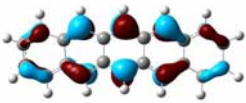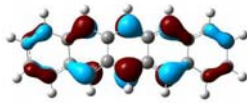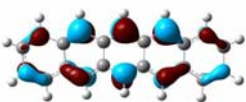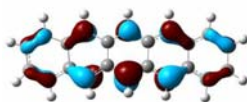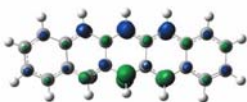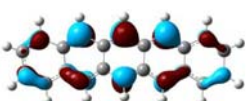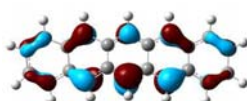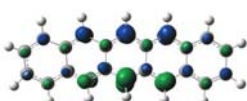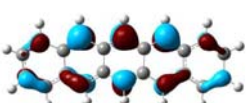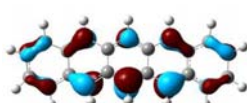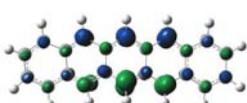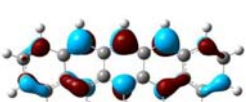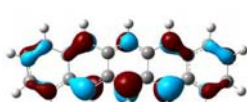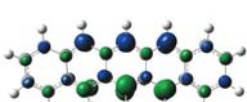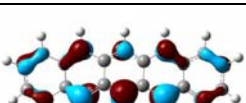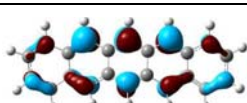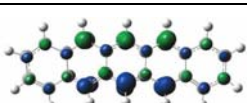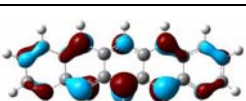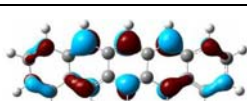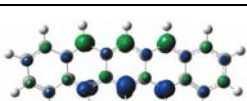
Time (fs)	SOMO (α)	SOMO (β)	Spin density distribution
648			
649			
650			
651			
652			

653			
654			
655			
656			
657			

657-672   CS state

673			
674			
675			
676			
677			
678			

679-695   CS state

696			
697			
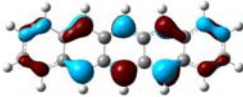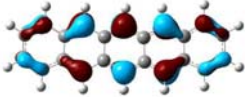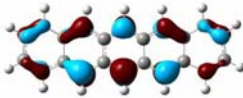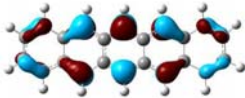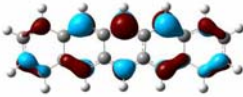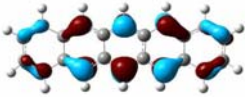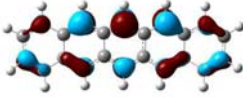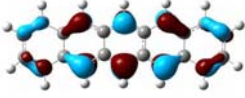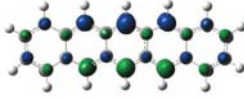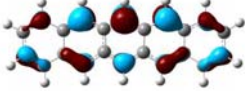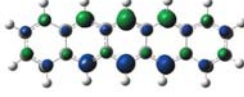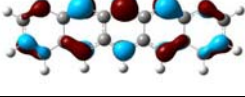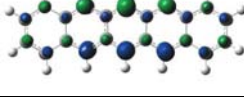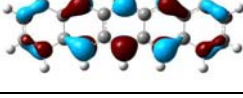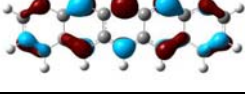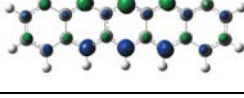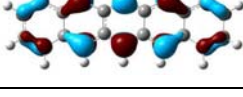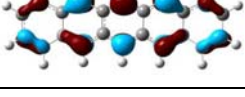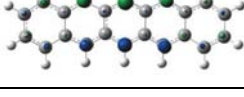
698			
699			
700			
701			
702-718 CS state			
719			
720			
721			
722			
723			
724			
725-739 CS state			
740			
741			
742			

743			
744			
745			
744-759 CS state			
760			
761			
762			
763			
764			
765			
766			
767			
768			
769-781 CS state			
782			

783			
784			
785			
786			
787			
788			
789			
788-805 CS state			
806			
807			
808			
809			
810			
811			
812-829 CS state			
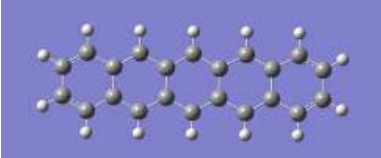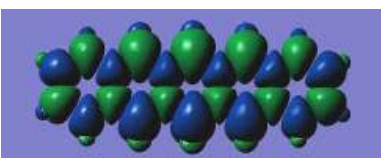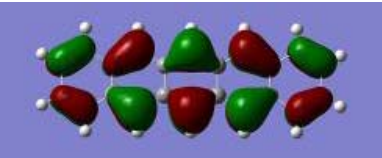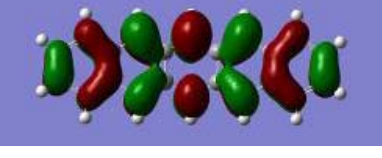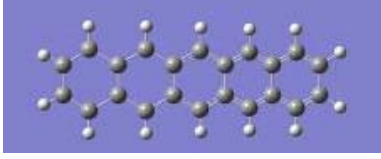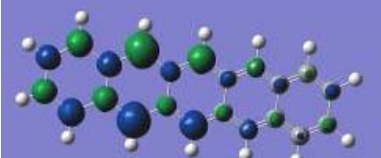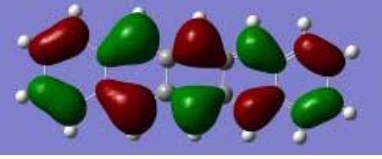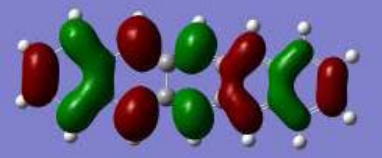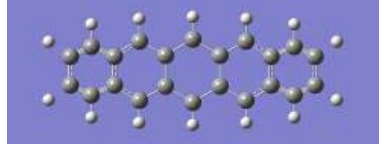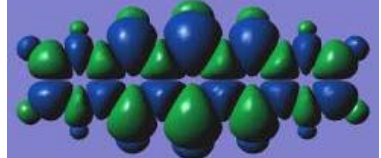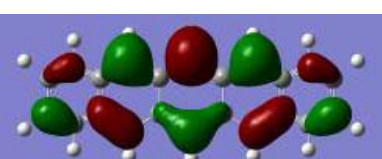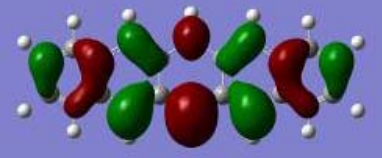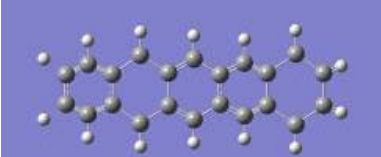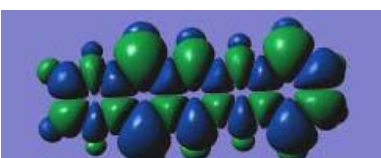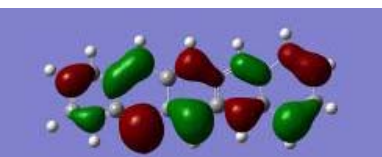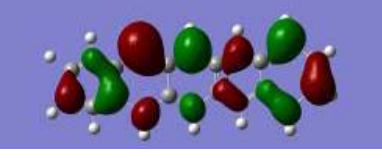
830			
831			
832			
833			
1716			
1717-1776 CS state			
1776			
1777			
1778			
1779			
1780			
1781			
1782			
1783			
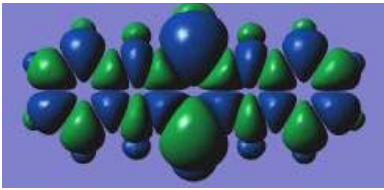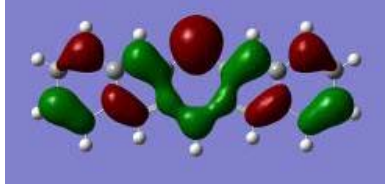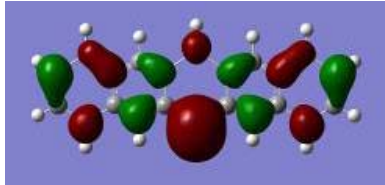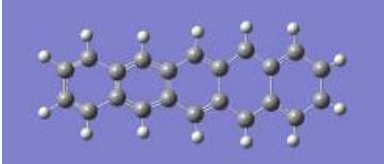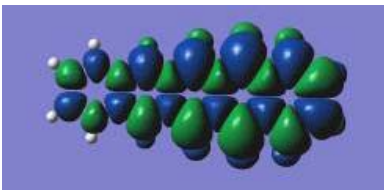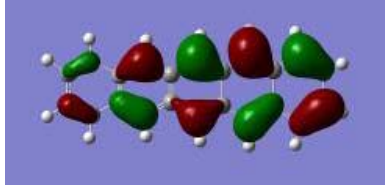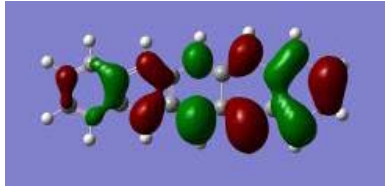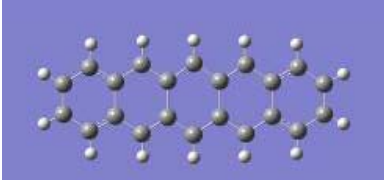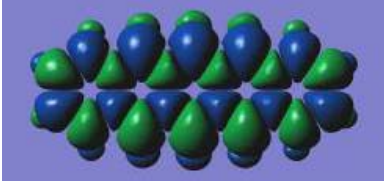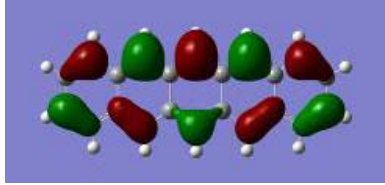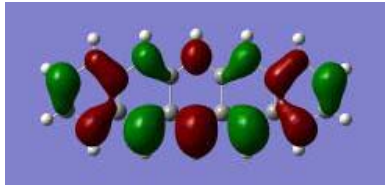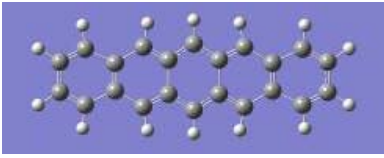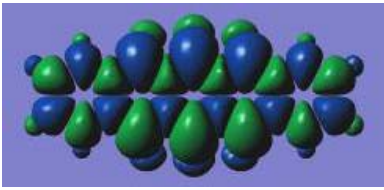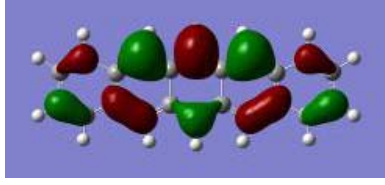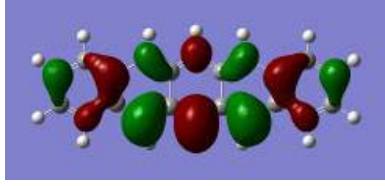
1784			
1785-1798 CS state			
1799			
1800			
1801			
1802			
1803			
1804			
1805			
1806-1823 CS state			
1824			
1825			
1826			
1827			
1828			
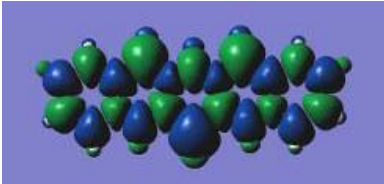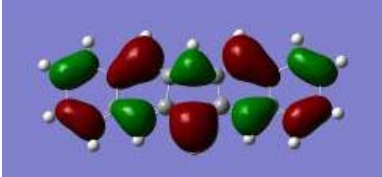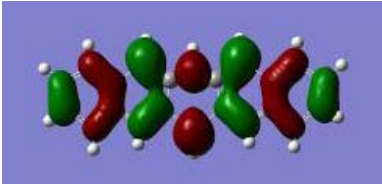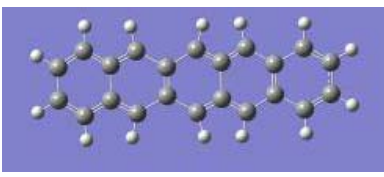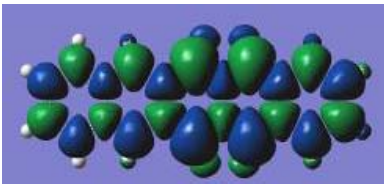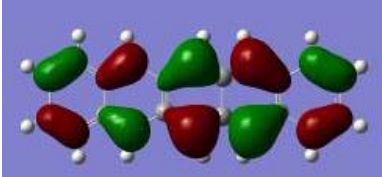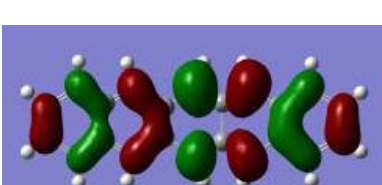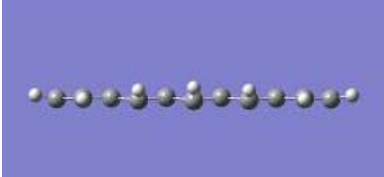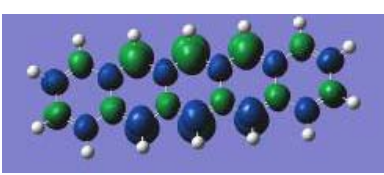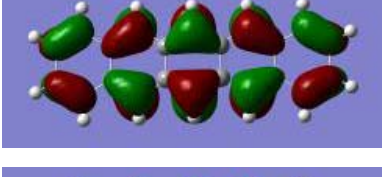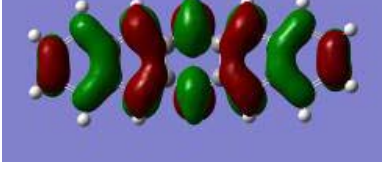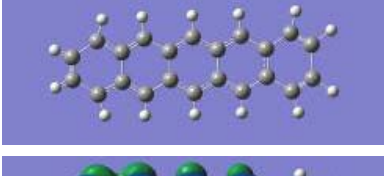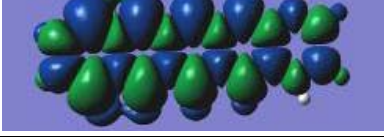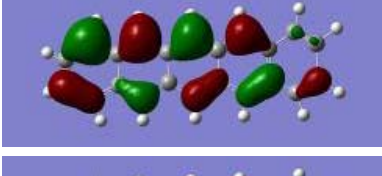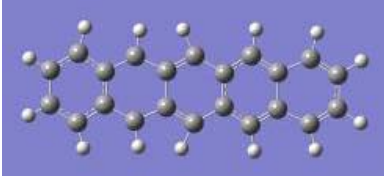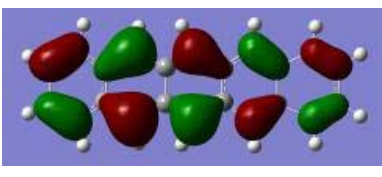
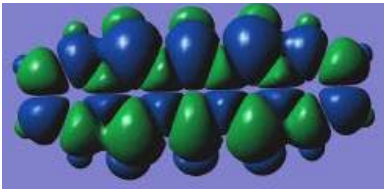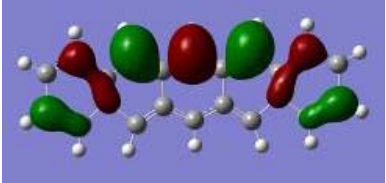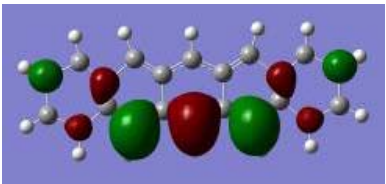| 1829			
1830-1788 CS state			
1889			
1890			
1891			
1892			
1893			
1894			
1895			
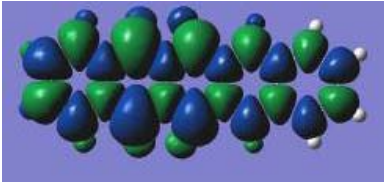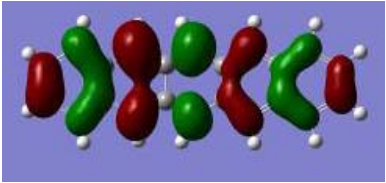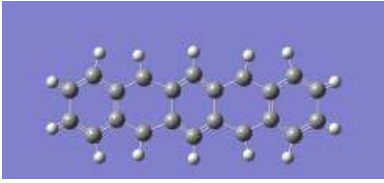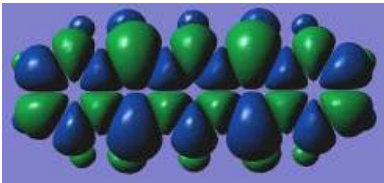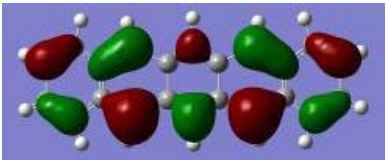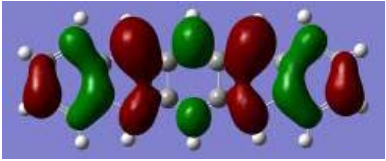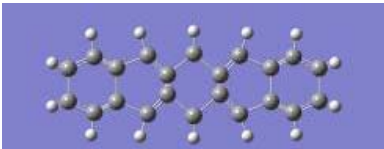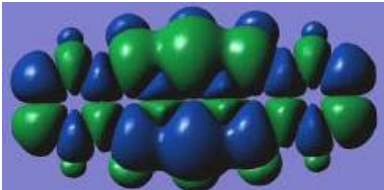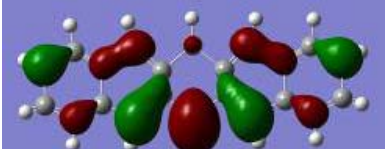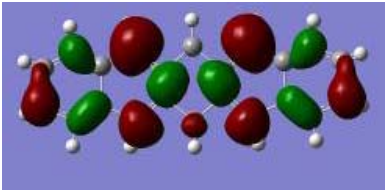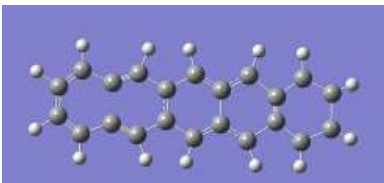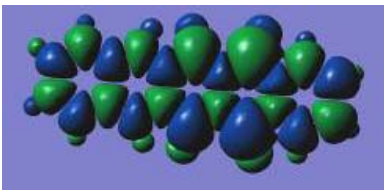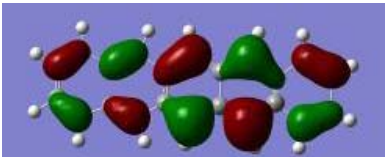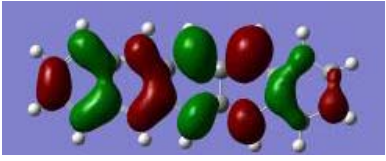
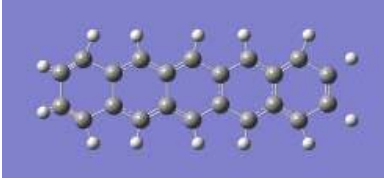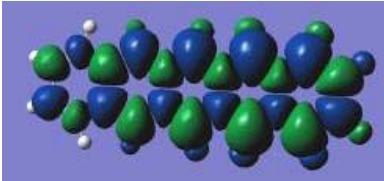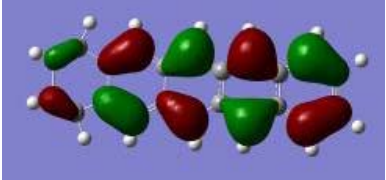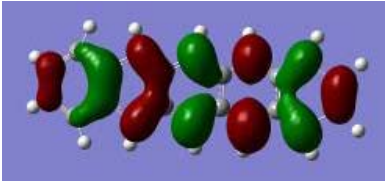## 9. Vibration-Caused Distorted Configurations and Their Diradical Character
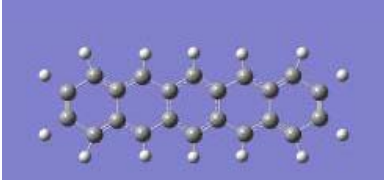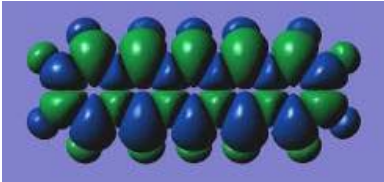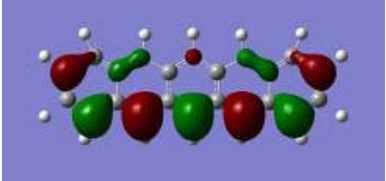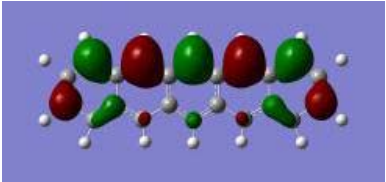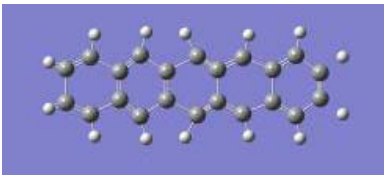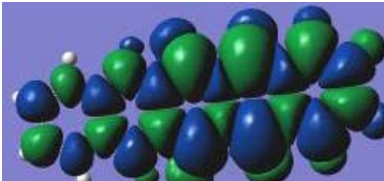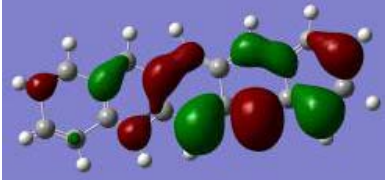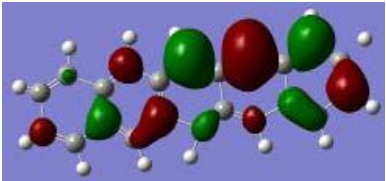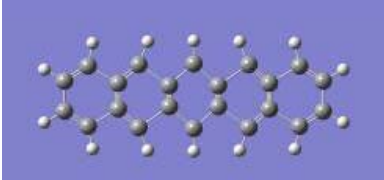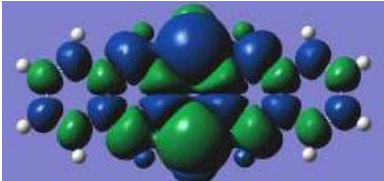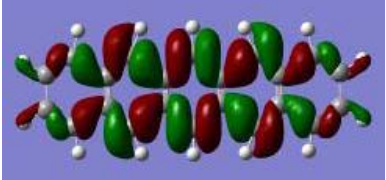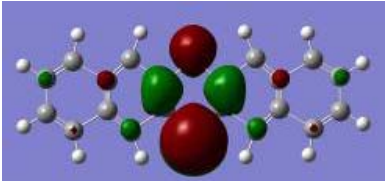
Table S12. 26 vibrational modes (the numbers in parentheses are referred to the numberings in the original 102 vibrational modes) which lead to diradical character of pentacene and the corresponding IR frequencies (Freq/cm^{-1}), geometrical characters, HOMO-LUMO gaps (H-L gap, eV) of the closed-shell singlet states, T-S gaps between the closed-shell singlet and triplet states (E(triplet)-E(singlet), kcal/mol), T-BS gaps between the broken-symmetry (BS) singlet and triplet states (E(triplet)-E(BS), kcal/mol), and $\langle S^2 \rangle$ values, SOMO (α,β), spin densities of the BS states of the mode-distorted pentacene configurations. Note that the distorted configuration denotes its largest distortion for each vibrational mode.
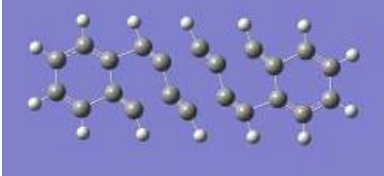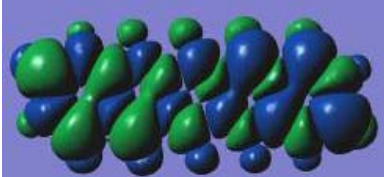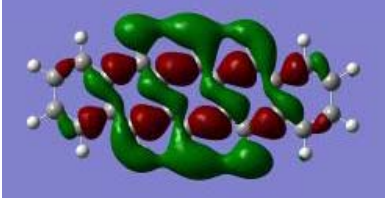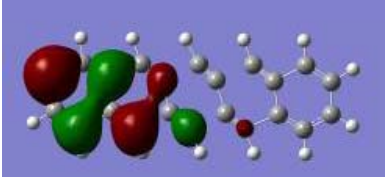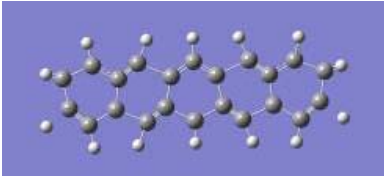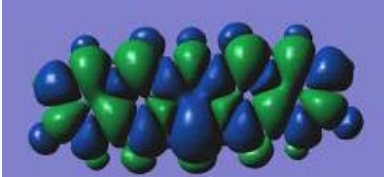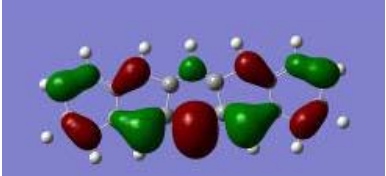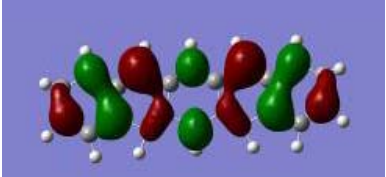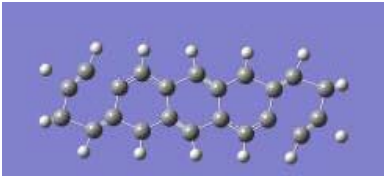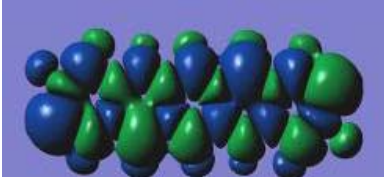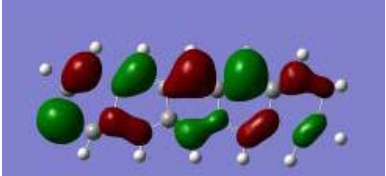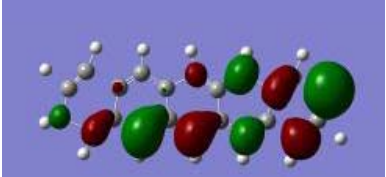
Modes Freq	H-L gap T-S gap T-BS gap $<S^2>$	Vibration-Induced Distortion Character (upper) BS State Spin Densities (lower)	BS State SOMO (α, upper) SOMO (β, lower)
1. (9) 263.25	2.008 17.81 17.83 0.0889		
2. (19) 490.10	2. 128 19.67 19.67 0.0002		
3.(24) 614.76	1.933 10.98 12.20 0.5052		
4.(25) 637.37	1.919 9.85 12.10 0.7054		

5.(26) 644.89	1.735 -1.99 5.86 0.8535		
6.(29) 745.99	1.950 13.55 14.08 0.3585		
7.(33) 762.86	1.700 10.11 11.24 0.5469		
8.(36) 796.76	1.707 6.36 8.37 0.6200		

9.(37) 835.17	2.090 18.03 18.04 0.0622		
10.(42) 891.14	2. 123 17.14 17.16 0.0675		
11.(47) 930.20	2.056 18.42 18.42 0.0165		
12.(53) 1020.13	1.715 8.48 10.20 0.6109		
13.(64) 1256.43	2.092 16.90 16.93 0.0910		

14.(69) 1337.79	1.929 15.24 15.75 0.3884		
15.(72) 1420.93	0.746 -28.22 1.84 1.2254		
16.(75) 1435.85	2.089 15.35 15.59 0.2437		
17.(76) 1442.37	0.933 -13.06 2.35 1.1125		

18.(78) 1482.12	2.051 17.99 18.01 0.0640		
19.(79) 1498.04	1.210 -0.10 7.23 1.1300		
20.(80) 1547.84	1.503 -2.42 4.15 0.8794		
21.(81) 1563.91	2.652 14.99 17.03 0.4631		

22.(85) 1640.76	0.573 -16.53 0.32 1.0523		
23.(86) 1645.43	1.880 9.02 11.09 0.6501		
25.(87) 1676.71	1.701 9.12 13.59 1.0236		
26.(88) 1678.56	1.368 -5.35 7.19 1.4610		